Effect of Pt/alumina catalyst preparation method on sensing performance of thermoelectric hydrogen sensor

Y. CHOI, K. TAJIMA, W. SHIN*, N. IZU, I. MATSUBARA, N. MURAYAMA
National Institute of Advanced Industrial Science and Technology, Nagoya 463-8560, Japan
E-mail: w.shin@aist.go.jp

Published online: 3 March 2006

We fabricated three different Pt/alumina catalysts for micro-thermoelectric hydrogen sensor (micro-THS). In the three Pt/alumina catalysts, two were prepared by impregnation of a commercial alumina with an aqueous solution of platinum (IV) chloride pentahydrate, and the third was prepared by impregnation of commercial alumina and nano-Pt with isobornyl acetate solution. To fabricate the micro-THS, the three Pt/alumina catalysts were integrated on thin membrane of the micro-THS, and its hydrogen sensing properties were investigated. The micro-THS with nano-Pt loaded alumina catalyst showed better sensing performance than those with Pt/alumina catalysts prepared by an aqueous solution of platinum (IV) chloride pentahydrate, because of effectively dispersed nano-Pt metal grain on the surface alumina grain observed by TEM. Its voltage signal was 15.7 mV for hydrogen concentration of 1% in dry air at catalyst temperature of 100°C.

1. Introduction

Hydrogen sensors have been fabricated by many researchers based on various operating principles [1–6]. Among them, the thermoelectric hydrogen sensor (THS) is one of the promising candidates for hydrogen leak alarm system because of its simple structure, reliable working principle, and sensing performance for wide-range of hydrogen concentrations. The THS using a thermoelectric effect was first demonstrated by McAleer *et al.* [5], and its working principle is as follows. When hydrogen gas was introduced into a catalyst, heat energy was generated on the catalyst surface due to the oxidation of hydrogen gas. This heat energy was converted to voltage signal through a thermoelectric layer. On the other hand, sensing performance of the THS can be largely improved by modifying device configurations and by changing the different thermoelectric materials. We have reported sensing properties of both bulk-THS and micro-THS [7–13]. Catalyst and thermoelectric layer in these THS are very important to make a sensor of high performance. The micro-THS was fabricated by several processes including the deposition of thermoelectric layer, the etching of substrate, the lift-off of micro-heaters, electrode lines, and the integration of the catalyst. By the micro-heater in the membrane, its power consumption with single membrane was greatly reduced compared to bulk-THS. Moreover, the structure of catalyst including the particle size, film thickness, and surface morphology are closely related to its sensing performance. Especially, the thick-film ceramic catalyst is expected to have the advantages of high sensitivity and long-term stability.

In the present work, the SiGe thin film thermoelectric pattern and the Pt-loaded on alumina (Pt/alumina) were used as a thermoelectric layer and a catalyst, respectively for the micro-THS. The paste of the Pt/alumina catalyst was deposited on the thin dielectric membrane of the micro-THS using a dispenser technique. This technique has the advantages of no mask patterning, precise positioning, and non-contacting. The purpose of this work is to investigate effects of catalyst preparation methods on hydrogen sensing performance, and the crystalline phases and micro-structures of the Pt/alumina catalysts were investigated in detail.

2. Experimental

We have prepared the Pt-loaded on alumina (Pt/alumina) catalysts by three different procedures. Flow chart of catalyst preparation is shown in Fig. 1. The Pt/alumina catalyst of the first method (Type I) was prepared by impregnation

*Author to whom all correspondence should be addressed.
0022-2461
DOI: 10.1007/s10853-006-7154-y

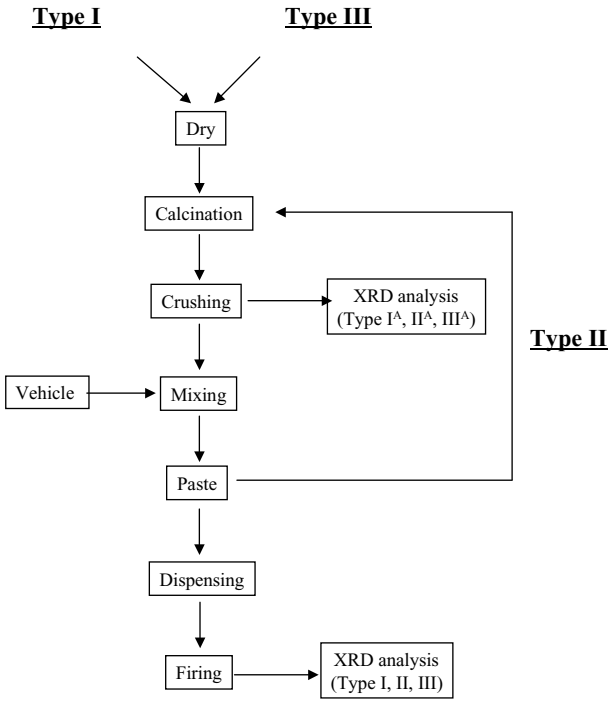

Figure 1 Preparation procedures of three different Pt/alumina catalysts by impregnation method.

of a commercial alumina powder with an aqueous solution of platinum (IV) chloride pentahydrate. The slurry was stirred at 100°C for 30 min, and then was dried at 120°C for 2 h in air. It was calcined at 300°C for 2 h. Before it was integrated on the micro-device, it was mixed with an organic vehicle to make ceramic pastes. The organic vehicle was a conventional dispersant which prepared a blend of terpineol and ethyl cellulose. The Pt/alumina catalyst of the second method (Type II) was prepared by the same impregnation method to the Type I until the process of preparation of the ceramic paste, as shown in Fig. 1. The ceramic paste was fired at 300°C again to get a powder of the Pt-loaded alumina. This catalyst powder was mixed again with organic vehicle. The Pt/alumina catalyst of the third method (Type III) was prepared by impregnation of the commercial alumina powder and nano-size Pt particles dispersed with isobornyl. Next procedures were carried out as the same way as Type I, as shown in Fig. 1. The Pt content in all three Pt/alumina catalysts was 10 wt% and the alumina powder was alpha-Al_2O_3 of 100 nm size.

Sub-millimeter size drop of the ceramic paste was deposited on the thin membrane of the micro-THS device using the dispenser technique with a CAD-Robot system (short mini-Musashi). After this integration of the ceramic paste on the thin membrane of the micro-THS, it was heated to remove the organic vehicle in air at 300°C.

Fig. 2 shows a photograph of the micro-THS (Type III, $5 \times 5 \times 0.35$ mm^3) with single membrane. The diameter and the thickness of a circular catalyst deposited on the membrane were 0.8 mm and average 13.4 μm, respectively. The backside silicon substrate of the membrane (1.1×2.4 mm^2) was etched away using KOH solutions. The membrane was heated up using the Pt-line heaters. The heater electrodes are ① and ③ in Fig. 2. For the microfabrication of micro-THS, the process details of the thermoelectric layer, the etching of backside silicon substrate by KOH solutions, the heaters, and the electrodes were reported previously [12].

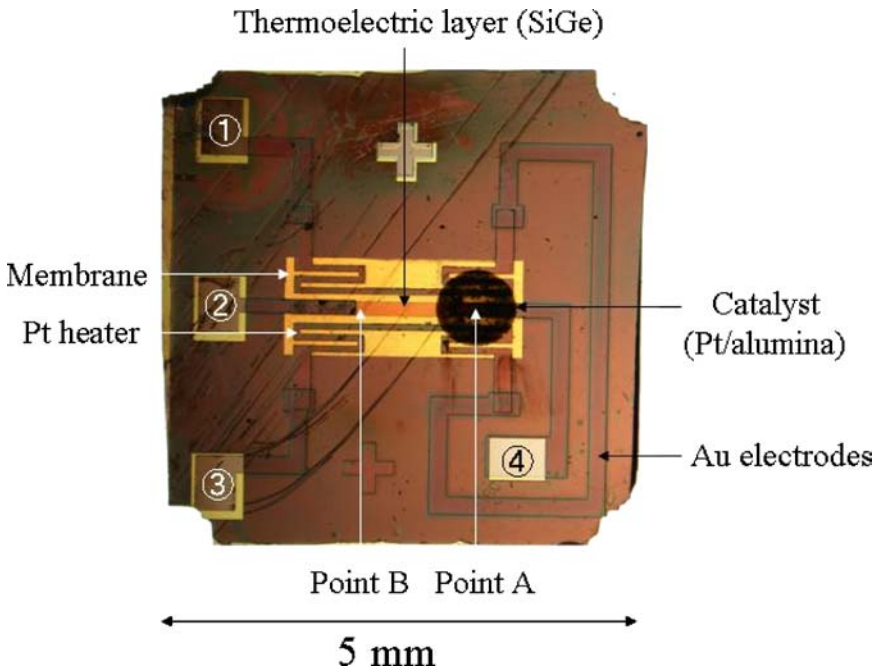

Figure 2 Photograph of micro-THS with Pt/alumina catalyst (Type III), which was integrated by a dispenser method. Heater electrodes are ① and ③. Thermo-voltage electrodes are ② and ④.

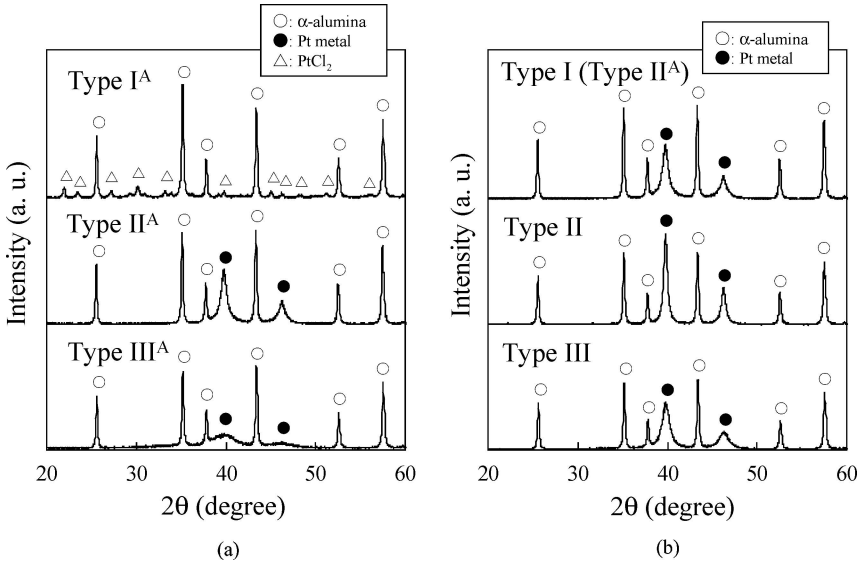

Figure 3 XRD patterns of three Pt/alumina catalysts. The peak patterns of alumina (◯), Pt metal (•), and $PtCl_2$ (△) are indicated. (a) Before catalysts of Type I, Type II and Type III were deposited on the micro-THS, (b) After catalysts of Type I^A, Type II^A and Type III^A were fired with a vehicle.

A gas flow system with a test chamber was used to investigate hydrogen sensing properties. When hydrogen gas was introduced into the test chamber, the heat was generated on the catalyst surface due to the oxidation of hydrogen gas. That is, a temperature difference was generated between the catalyst (hot-side, point A in Fig. 2) and the SiGe layer (cold-side, point B in Fig. 2) in membrane and it was converted to voltage signal by the thermoelectric layer. By the Seebeck effect, voltage signal is linearly proportional to temperature gradient between the hot side and the cold side. The thermo-voltage electrodes are ② and ④ in Fig. 2 An IR camera was used to monitor the surface temperature of catalyst and SiGe layer through a sapphire top window of the test chamber. The hydrogen sensing performance of micro-THS was evaluated by measuring the voltage change or the temperature difference between catalyst and SiGe layer. The test procedure is as follows: a dry air was flowing into the test chamber (inner volume: $44 \times 48 \times 13\ mm^3$) for 60 s. After that, the flow was switched from dry air to hydrogen/air mixture for 240 s. The Hydrogen/air mixture was changed again to the dry air. The flow rate was 100 cc/min. The gas flow and data acquisitions were automatically controlled by a computer.

The crystalline phase and micro-structure of the catalysts were investigated by X-ray diffraction (XRD) and Transmission Electron Microscopy (TEM, JEOL, JEM-2010), respectively.

3. Results and discussion

The XRD patterns of three powder catalysts are shown in Fig. 3a, and the XRD patterns of deposited and fired catalysts are shown in Fig. 3b. Before the catalyst of Type I was mixed with the organic vehicle (Type I^A), its crystalline phase was $PtCl_2$/alumina. When the $PtCl_2$/alumina was fired with the organic vehicle, it transformed into Pt/alumina (Type I in Fig.3b). The color of the $PtCl_2$/alumina and the Pt/alumina were brown and black, respectively. It means that chlorides in the $PtCl_2$/alumina were deleted by the firing treatment, and $PtCl_2$/alumina was changed into Pt/alumina. The organic vehicle seems to work as a reducing agent during the firing process. Therefore, Type I and Type II on the micro-THS devices were integrated as crystalline phases of $PtCl_2$/alumina and Pt/alumina, respectively before the final firing. When the Pt/alumina catalysts such as Type II^A and Type III^A were used as a starting material, intensities of the Pt XRD peaks were increased by the firing with the organic vehicle. In the Pt/alumina catalysts, Pt grain size was calculated from the XRD peak broadening analysis using Williamson-Hall equation [14]. The grain size of Pt metals in the catalysts of Type I, Type II and Type III were estimated to be 11.6, 17.1 and 10.7 nm. Marecot et al reported that chlorides remaining on the catalyst surface could block active sites for alkane oxidation on Pt [15], and concluded that the removal of the chlorine from the catalyst surface by water produced during the total combustion of hydrocarbons would be responsible for the increase in activity after successive oxidation cycles. In this work, we could not observe the chlorine element in the three catalysts of Type I, Type II and Type III from EDX analysis as well as XRD measurements.

Fig. 4 shows the TEM images of Type I, Type II, and Type III. The dark features in TEM images are Pt grains. The Pt grains were attached on the alumina surface. There was no difference in the size of Pt metal grains of the catalyst of Type I, Type II and type III, which was ca. 10 nm. However, the dispersion of Pt particles was different. Large agglomerations of Pt grains with the size of ca. 100 nm were also observed in Type I and Type II, but agglomerations of Pt grains with the size of ca. 30 nm were observed in Type III. That is, Type III was prepared with effectively dispersed Pt grains, compared to Type I or Type II. Difference in the Pt grain size between XRD

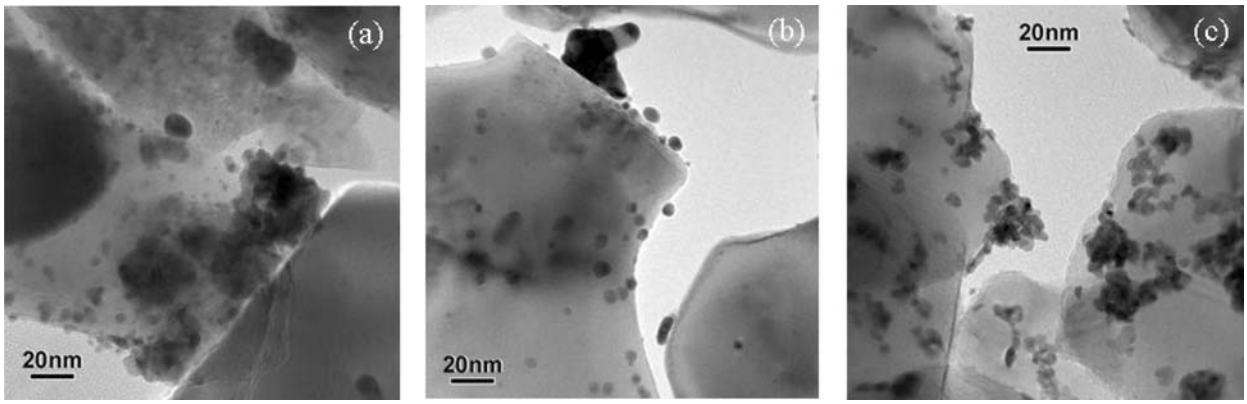

Figure 4 TEM images of Pt/alumina catalysts (× 100,000), (a) Type I, (b) Type II, (c) Type III.

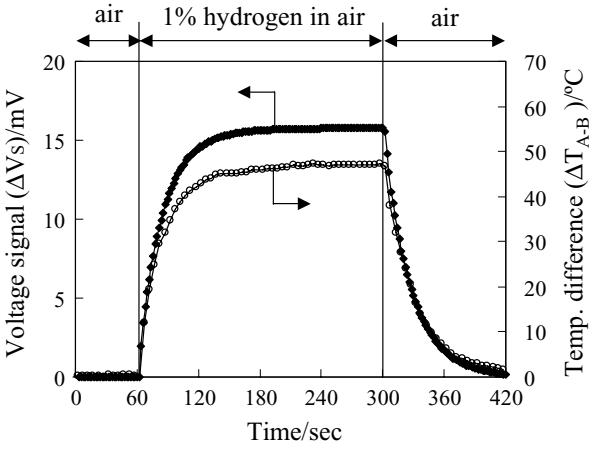

Figure 5 Typical hydrogen response of micro-THS with catalyst of Type III for hydrogen/air mixture of 1%. Gas flow rate: 100 ccm. Catalyst temperature: 100°C.

measurements and TEM observations might be related to the Pt agglomerations observed in the TEM image.

After the three catalysts were deposited on the micro-THS devices, the hydrogen sensing properties of the micro-THS devices were investigated. Fig. 5 shows the typical hydrogen responses (ΔV_S and ΔT_{A-B}) of the micro-THS with the catalyst of Type III for 1% hydrogen in dry air at the catalyst temperature of 100°C. The ΔV_S is the difference of voltage signal of the device before and after introduction of hydrogen/air mixture. The ΔT_{A-B} is equal to $\Delta T_A - \Delta T_B$, where ΔT_A and ΔT_B mean the temperature changes on the catalyst surface and SiGe layer before and after introduction of hydrogen/air mixture. When the micro-THS was exposed to hydrogen/air mixture gas, the ΔV_S and ΔT_{A-B} increased due to the heat of hydrogen oxidation on the catalyst. At the catalyst temperature of 100°C, the saturated V_s for the micro-THS devices with the catalysts of Type I, Type II, and Type III were 7.3, 10.9 and 15.7 mV, respectively. The saturated ΔT_{A-B} for micro-THS devices with the catalysts of Type I, Type II, and Type III were 28.1, 33.5 and 47.3°C, respectively. From these results, it was confirmed that voltage signal was proportional to the temperature gradient between the catalyst (hot side) and the SiGe layer (cold side), due to the thermoelectric effect. In the case of the micro-THS with Type III, from the values of ΔT_{A-B} and V_s for 1% hydrogen/air mixture gas at catalyst temperature of 100°C, the $V_s/\Delta T_{A-B} = 0.332$ mV/K. The summary of the $V_s/\Delta T_{A-B}$ for three micro-THS devices is shown in Table I The $V_s/\Delta T_{A-B}$ of Type II and Type III was almost same, while the $V_s/\Delta T_{A-B}$ of Type I was low compared to that of the micro-THS devices with Type II or Type III. Difference of the $\Delta V_s/\Delta T_{A-B}$ between micro-THS with Type I and micro-THS with Type II or Type III might be related to the catalyst thickness on the membrane as shown in Table I. The thickness of the catalyst increases with increasing the viscosity of catalyst. When the thickness of the catalyst is thick, it is reasonably considered that the temperature of catalyst surface is low compared to that of catalyst bottom, resulting in the low $V_s/\Delta T_{A-B}$. However, these calculated $V_s/\Delta T_{A-B}$ values are 2.3 (Type I) or 2.9 (Type II or Type III) times highe than that of the measured value (0.115 mV/K) [16], while that of the micro-THS with Pt thin film is in good agreement with the measured value as shown in Table I. It was

TABLE I Summary of the results for micro-THS devices with three Pt/alumina thick ceramic catalysts and micro-THS with Pt thin film catalyst.

	Type I	Type II	Type III	Pt Thin film [Ref.16]
Voltage signal ΔV_s(mV)	7.3	10.9	15.7	0.358
Temperature diff. ΔT_{A-B}(K)	28.1	33.5	47.3	3.41
$\Delta V_s/\Delta T_{A-B}$(mV/K)	0.260	0.325	0.332	0.105
Average Catalyst thickness (μm)	16.4	14.0	13.4	0.3
Catalyst diameter (mm)	0.8	0.8	0.8	15×15 (mm^2)
Viscosity of catalyst paste (cps)	3,000	2,000	1,700	–

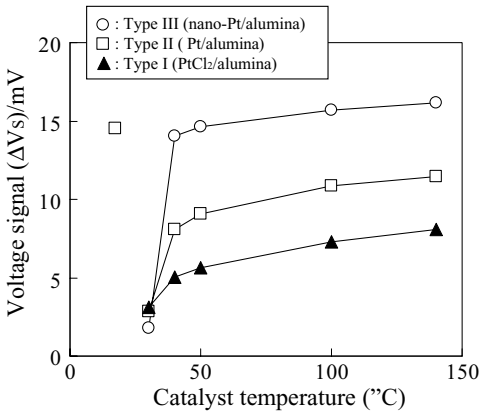

Figure 6 The changes of the voltage signals as a function of catalyst temperatures. Hydrogen concentraton: 1%, Gas flow rate: 100 ccm.

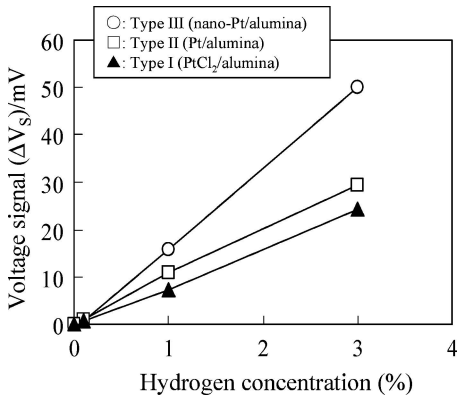

Figure 7 The changes of the voltage signals as a function of hydrogen concentration. Catalyst temperature: 100°C. Gas flow rate: 100 ccm.

suggested that the temperature of catalyst surface is different with that of catalyst bottom, which was contacted to the thermoelectric layer. From the measured $V_s/\Delta T_{A-B}$ and V_s values, the temperature of the catalyst bottom for the three micro-THS devices was estimated to be 63.5, 94.8, and 136.5°C. The expected temperature of catalyst bottom is directly related to the sensing performance. Because the grain size of Pt metal in the three catalysts were almost same, the way of dispenser of the Pt/alumina catalysts would induce this large difference. With effectively dispersed nano-Pt/alumina catalyst, the micro-THS with Type III shows higher sensing performance than those of micro-THS devices with the catalysts of Type I or Type II.

Fig. 6 shows the changes of voltage signal as a function of the catalyst temperatures in micro-THS with the three catalysts. The voltage signal (ΔV_s) increased with the catalyst temperature. When the catalyst temperature was over 40°C, the ΔV_s of micro-THS with Type III was the highest value among the micro-THS devices with three catalysts. The V_s of all the micro-THS devices became low abruptly and were was almost same when the catalyst temperature was 30°C for 1% hydrogen. This low performance at 30°C cannot be explained by difference of the dispersion of Pt metals on the alumina grain. It should be further investigated to clarify the reasons.

Fig. 7 shows the changes of voltage signals as a function of the hydrogen concentrations in air when the catalyst temperature is 100°C. For the micro-THS with three catalysts, voltage signal increased linearly with the hydrogen concentration. A linear relation between voltage signals and hydrogen concentrations was observed in the hydrogen concentration range of 50 ppm -3%. From these results of Figs. 6 and 7, the ΔV_s of the micro-THS with the catalysts of Type III was higher than those of the devices with the catalysts of Type I or Type II. The high performance of the micro-THS with Type III is closely related to the high dispersion of Pt metals on the alumina based on the TEM observations, as discussed above. For this result, we can conclude that the hydrogen sensing performance can be improved by the preparation methods of the catalysts.

4. Conclusions

Integration of the various Pt/alumina catalysts on thin single membrane of micro-thermoelectric hydrogen sensor (micro-THS) was successfully carried out by the dispenser technique. Among the three different Pt/alumina catalysts of the fixed Pt content in the Pt/alumina of 10 wt%, two were prepared by impregnation of a commercial alumina with an aqueous solution of platinum (IV) chloride pentahydrate, and the third was prepared by mixing of commercial alumina and nano-Pt with isobornyl acetate solution. Hydrogen sensing property is very dependent upon the preparation methods of the catalysts, which can influence the Pt dispersion on the alumina. The voltage signal of the micro-THS with Nano-Pt loaded alumina was the highest among the micro-THS devices with three catalysts due to the effectively dispersion of Pt metal on the alumina. The voltage signal of micro-THS with nano-Pt loaded alumina was 15.7 mV for the hydrogen concentration in air gas of 1 % at the catalyst temperature of 100°C. The hydrogen sensing performance of micro-THS with three type catalysts were as follows: Nano-Pt loaded on alumina (Type III) > Pt/alumina (Type II, starting material: Pt/alumina) > Pt/alumina (Type I, starting material: $PtCl_2$/alumina).

Acknowledgments

This work was supported by New Energy and Industrial Technology Development Organization (NEDO), Japan.

References

1 I. LUNDSTROM, S. SHIVARAMAN, C. SVENSSON and L. LUNDKVIST, *Appl. Phys. Lett.* **26** (1975) 55.
2 K. DOBOS, R. STROTMAN and G. ZIMMER, *Sens. Actuators* **4** (1983) 593.
3 J. P. HALL, R. W. WHATMORE and F. W. AINGER, *Ferroelectrics* **54** (1984) 551.
4 M. A. BUTLER, *Phys. Lett.* **45** (1984) 1007.

5 J. F. MCALEER, P. T. MOSELEY, P. BOURKE, J. O. NORRIS and R. STEPHAN, *Sens. Actuators* **8** (1985) 251.
6 H. BALTES, *ibid. A* **56** (1996) 179.
7 W. SHIN, K. IMAI, N. IZU and N. MURAYAMA, *Jpn. J. Appl. Phys.* **40** (2001) L1232.
8 M. MATSUMIYA, W. SHIN, N. IZU and N. MURAYAMA, *Sens. Actuators B* **93** (2003) 309.
9 W. SHIN, M. MATSUMIY, N. IZU and N. MURAYAMA, *ibid.* **93** (2003) 304.
10 K. TAJIMA, F. QIU, W. SHIN, N. SAWAGUCHI, N. IZU, I. MATSUBARA and N. MURAYAMA, *Jpn. J. Appl. Phys.* **43** (2004) 5978.
11 W. SHIN, K. TAJIMA, Y. CHOI, N. IZU, I. MATSUBARA and N. MURAYAMA, *Sen. Actuators B*, **108** (2005) 455.
12 K. TAJIMA, Y. CHOI, W. SHIN, N. IZU, I. MATSUBARA and N. MURAYAMA, *Key Enging. Mater*,. **301** (2006) 273.
13 Y. CHOI, K. TAJIMA, W. SHIN, N. IZU, I. MATSUBARA and N. MURAYAMA, *Appl. Catal. A*, **287** (2005) 19.
14 G. K. WILLIAMSON and W. H. HALL. *Acta Metall.* **1** (1953) 22.
15 P. MARECOT, A. FAKCHE, B. KELLALI, G. MABILON, P. PRIGENT and J. BARBIER, *Appl. Catal. B* **3** (1994) 283.
16 K. TAJIMA, F. QIU, W. SHIN, N. IZU, I. MATSUBARA and N. MURAYAMA, *Sen. Actuators B*, **108** (2005) 973.

Received 7 February
and accepted 27 June 2005